Knock analysis in the crank angle domain for low-knocking cycles detection

Author, co-author (Do NOT enter this information. It will be pulled from participant tab in MyTechZone)

Affiliation (Do NOT enter this information. It will be pulled from participant tab in MyTechZone)

Abstract

Knock is an abnormal phenomenon with in-cylinder pressure oscillations, which must be avoided to protect the engine from damage and to avoid excessive noise. Conventional control algorithms delay the combustion with the spark to avoid high knocking rates but reduce the thermal efficiency and restricts the performance of a spark ignition engine. The detection and characterization of low-knocking cycles might be used for improving knock control algorithms, however, it is a challenging task, as normal combustion also excite the different resonance modes and might be confused with knock.

Most of the methods found in literature for knock detection use 0-Dimensional indicators, regardless of the angular evolution of the pressure oscillations. In this paper, the in-cylinder pressure oscillations evolution during the piston stroke is analyzed by using various time-frequency transformations. The analysis highlights the need of a new criteria for knock detection, which must take into account the intensity of the oscillations but also the crank angle location where they take place. A new definition of knock is proposed by using resonance to design an indicator of the pressure resonance evolution and by assuming constant volume combustion at knock to determine the minimum oscillation required for end-gas auto ignition detection as a function of the crank angle location. Several experimental tests with an EURO VI SI engine are used for illustration and validation purposes. A conventional knock control algorithm was used for comparing the new knock event definition with the classical MAPO definition, being the new indicator able to improve the performance of the controllers by giving more information about knock and introducing lower spark advance (SA) variability.

Introduction

Knock is an abnormal combustion phenomenon of spark ignition engine (SI) associated with the auto ignition of a portion of the fuel-air mixture ahead of the propagating flame front [1, 2]. According to Internal combustion engine fundamentals by Heywood [3], in a normal SI combustion event, the flame propagates from the spark plug to the opposite end of the combustion chamber. Under knocking conditions, the end-gas is auto-ignited, the energy released from the end-gas may cause a local high pressure, and this rapid combustion produces shock waves, which are propagated across the cylinder and heavily excites the cylinder resonant modes. When knock occurs, high-frequency pressure oscillations can be observed, and the pressure waves are propagated across the cylinder.

Knock reduces the engine efficiency, produces vibration noise, and heavy knock might cause damage to the engine [4, 5]. Knock remains one of the major barriers to further improve the thermal efficiency of SI, usually operated at knock-limited spark advance to achieve possibly maximum efficiency [6].

One of the main control parameters in SI engines is the SA. Retarding the spark timing the combustion is delayed, preventing gases from reaching very high temperature and pressure conditions, and hence, increasing the time required for auto ignition and avoiding knock [3].

Knocking detection is crucial because it determines engine durability, fuel consumption, and also characterize the knock controller performance: a false detection of knock lowers the engine efficiency, while any detection failure might lead to engine damage [7].

There are many methods used to detect knock, they can be divided in those based on a direct detection and the methods based on an indirect detection. The first ones are based on the measurement of the in-cylinder pressure oscillations, while indirect methods use alternative sensors where knock phenomenon might be also distinguished, e.g. cylinder block vibration. Due to its simplicity, vibration measurement is largely employed in industry. However, the quality of knock detection is often affected by noise related [1]. Cylinder pressure is the most important classical diagnostic in engine studies, is directly affected by knock and provide reliable information, for that reason it is more accurate for knock detection and largely employed in laboratory tests [9,10]. The difference between the in-cylinder pressure signal and the knock sensor for low knocking cycles detection is analyzed in Appendix A.

Some methods based on in-cylinder pressure use a high-pass or a band-pass filter to analyze the oscillation in the time domain: MAPO (Maximum Amplitude of Pressure Oscillations) and IMPO (Integral of Modulus of Pressure Oscillations) are the most extended for knock detection. The first one computes the maximum absolute value of the filtered pressure signal, while the second one integrates the intensity of the fluctuations [10, 11]. Other methods are based on heat release analysis, by profiting from the fact that the combustion process of the knocking cycles introduces a peak in the heat release due to rapid combustion near the end of combustion (EOC), e.g. in [12] five heat transfer coefficient correlations are compared to find the most suitable to predict the knock occurrence, which can be used to improve the quantification performance. Other authors use the frequency domain to obtain indexes, some examples can be found in [13] with the discrete Fourier transform or in [14, 15] with discrete Wavelet transform.

Most of these indexes are 0-Dimensional, i.e. only one value is obtained per cycle that evaluates the oscillation intensity. This indicator is compared with a pre-settled threshold which is used to separate normal combustion from knocking combustion regardless the location in crank angle degree where the excitation takes place. In knocking cycles, the combustion process has two stages: a normal flame propagation induced by spark, which increases the in-cylinder pressure and a non-desired end-gas auto-ignition. In Bares et al. [16] a new knock event definition is proposed. This method consists in comparing the excitation of the cylinder resonance produced by auto ignition with that associated with combustion.

In order to reduce the knocking tendency of the engine, it is necessary to study the methods of knock detection. The objective of the present study is to develop an improved understanding of the phenomena occurring during the knock and to develop a new knock event definition by using a time frequency analysis of the in-cylinder pressure signal in various operating conditions. The angular evolution of the in-cylinder pressure oscillations is considered to detect low knocking cycles and avoid false knock detection. The new knock indicator proposed is compared with the MAPO indicator by using a conventional knock controller.

This paper is organized as follows: next section describes the experimental set-up and the tests performed. After, a time-frequency analysis is performed, followed by the analysis of several cycles, with and without knock, in order to characterize the knock phenomena. Once knock is characterized, a new knock event definition is proposed. Then, the online validation of the new knock indicator with a conventional knock controller is performed, and finally, the main conclusions of the work are collected.

Experimental set-up

A four-stroke SI engine was used to analyze knock and validate the new definition proposed. The specifications of the engine are shown in Table 1.

Table 1. Engine main characteristics.

Displaced volume	1300 cc
Stroke	81.2 mm
Bore	72 mm
Compression ratio	10.6:1
Combustion	SI
Number of cylinders	4
Fuel	Gasoline

The engine is coupled in a test bench with in-cylinder, intake manifold and exhaust manifold pressure sensors. Figure 1 shows an image of the control system of the engine, that includes an electronic control unit (ECU), which has been bypassed with an ETAS ES910 system for modifying the standard calibration. A prototyping system from National Instruments TM was used for acquisition, control, and diagnosis purposes. The system consists of:

- A PXI 6123 and PXI-6251 acquisition modules were used to acquire information from sensors with high sampling rate and 16-bit resolution, e.g. in-cylinder pressure sensor.
- A NI-9759 module was used with a PXI 7813R for programming in FPGA the full-pass control.
- A CAN interface module, PXI-8513, was used to communicate with the ES910 system.
- A PXI 8110 controller was used to compute the control strategy and to process, store and analyze all the information from the previous modules.

The variable geometry turbine (VGT) position was directly controlled with the FPGA by full-pass while the throttle valve position, the VVT, the spark advance, and the injected fuel were controlled through ECU by-pass, so not only the calibration but the complete control strategy can be modified with the prototyping system.

An optical encoder was used to provide the crank angle reference for the in-cylinder pressure collection with a sampling accuracy of 0.2 crank angle degree.

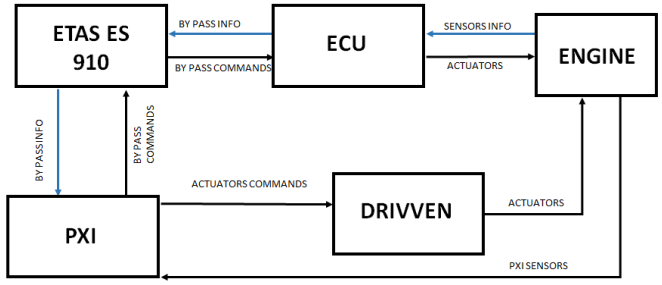

Figure 1. Control system of the engine.

During the experiments, the engine was tested at several operating conditions, by keeping the speed, the intake pressure and stoichiometric ratio constant. Two kind of experiments were performed for illustration and validation purposes:

- Steady state tests: Five steps of SA were performed at nine operating conditions, i.e. three different engine speeds,1500, 2000 and 3000 RPM, and three loads, 0.9, 1 and 1,1 bar of pressure in the intake manifold.
- Validation tests: SA was controlled by a conventional knock control using the traditional knock definition (MAPO > 0.4 bar) and the new knock event definition, with the engine running at 2000 RPM and 1 bar of pressure in the intake manifold.

All the analysis developed throughout the document was performed on one of the engine cylinders.

Time frequency analysis

The in-cylinder pressure signal is initially measured in the crank angle domain and transformed into the time domain according to the sampling accuracy (encoder resolution) and engine speed. The sampling frequency is calculated as:

$$F_s = \frac{360n}{60s_n} \quad (1)$$

Where n is the engine speed (RPM) and s_n is the sampling accuracy (deg/sample).

The in-cylinder pressure frequency can be divided by three components: low frequencies (f< 500 Hz) are associated to the movement of the piston, medium frequencies (0.3 < f < 2 kHz) to the maximum rate of pressure rise caused by combustion, and high frequencies (f>4 kHz) to the resonance of the chamber. Resonance in the piezoelectric pressure sensor and other noises can be also found at higher frequencies (f>50 kHz) [17].

The in-cylinder pressure signal in the time domain does not provide direct information of the resonant frequencies while the frequency analysis with a Fourier transform does not have crank angle resolution for the different phenomena. The short-time Fourier transform (STFT) provides precise frequency information with respect to the crank angle by windowing the pressure signal and sliding the window along different crank angle positions [14]. STFT is defined as:

$$P_{STFT}(t,f) = |F[p(\tau)h(\tau - t)]| \quad (2)$$

where $F[p(\tau)]$ is the fourier transform of the signal $p(\tau)$ and $h(\tau - t)$ is the window function.

Figure 2 analyses the pressure signal for a non-knocking, a low knocking, and high knocking combustion cycle, with the engine running in steady-state at 11.9 bar of indicated mean effective pressure (IMEP) and 2000 rpm of engine speed. In the left axis of the top plots, the evolution of the in-cylinder pressure (p) and the heat release rate (HRR) are shown normalized with their maximum values are shown. In the bottom plots the corresponding frequency spectrograms by using a Blackman-Harris window of 30 CAD are also included. More detail information about window functions can be found in Appendix B.

The theoretical resonant modes are plotted with dashed blue lines, while the crank angle position where 50% of the heat is released (CA50) is highlighted with a vertical red dashed line.

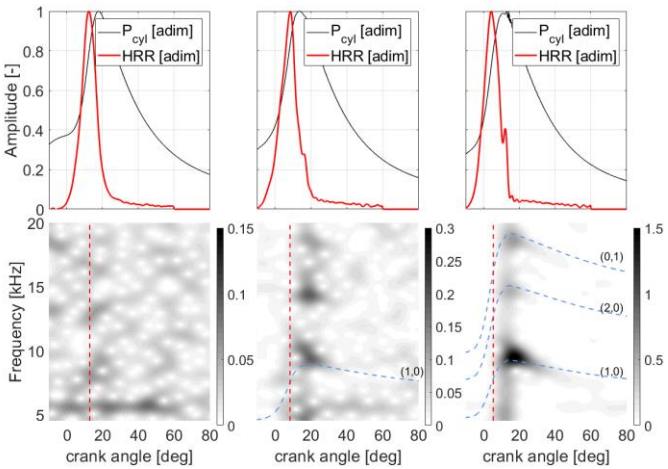

Figure 2. HRR and in-cylinder pressure (top plots) with their spectrogram (bottom plots) from three cycles; no-knocking cycle (left), low-knocking cycle (middle) and knocking cycle (right). Blue dotted lines represent the main resonant frequencies theoretically calculated. Operation point: 2000 rpm. Pint=1 bar.

Note that the scale of the frequency intensities at the spectrograms is different in the three cases. In the first case, i.e. no knock, the resonance of the combustion, which appears around 9 kHz, is hidden by a constant noise that appears slightly above 5 kHz and which is excited before combustion. In the other two cases, an abnormal increase in the heat release rate after combustion is observed, and the main frequency components excited at the spectrogram are those related with the resonant modes, excited by a local increase in heat release produced by autoignition.

In the first case (no knock MAPO 0.08 bar), left plots, have been obtained by processing a cycle with a Spark advance of 7 CAD, the second case (low knock MAPO 0.21 bar) has been obtained by setting the SA at 8 CAD, while the last case (knocking cycle MAPO 1.5 bar) has been obtained by using a spark timing at 11 CAD before top dead center (BTDC). Spark timing has a substantial effect in knock occurrence, and it is the most common control parameter to avoid it. Knock increases when spark timing is advanced because the greater the spark advance is, the longer the combustion takes place in the compression stage, where the pressure and temperature are increasing, and therefore, there is a greater probability of knock occurrence [18, 19].

The theoretical resonant frequency evolution can be estimated by a cylindrical chamber assumption. Draper solved analytically the wave equation assuming cylindrical contour conditions by using Bessel functions [20]. The specific frequencies depend on the excited resonant mode, combustion parameters, and cylinder geometry:

$$f_{ij} = a_s\sqrt{\frac{{B_{ij}}^2}{(\pi * D)^2} + \frac{g^2}{(2h)^2}} = \frac{a_s B_{ij}}{\pi D} \quad (3)$$

where the axial modes g are neglected near the TDC because the height is too low ($h \ll D$), D is the bore of the cylinder, a_s the speed of sound and B_{ij} are the Bessel constants related with the radial modes. The speed of sound can be calculated by measuring the trapped mass m, the in-cylinder pressure p, and estimating the instantaneous volume of the chamber V.

$$a_s = \sqrt{\frac{\gamma p V}{m}} \quad (4)$$

Where γ is the specific heat capacities ratio of the gases inside the cylinder, which can be approximated by dividing the gas mixture in three species, namely air, fuel, and burnt products, and modelled by polynomial expressions for the in-cylinder temperature such as suggested in [21].

The various resonant modes are tabulated in Table 2. The lowest mode (1,0) typically possesses most of the pressure oscillating energy in combustion engines, as higher frequencies are damped faster.

Equation 4 can also be written as a function of temperature (T) and the gas constant (R) as follows:

$$a_s = \sqrt{\gamma R T} \quad (5)$$

According to equation (5) and an engine of characteristics named in table 1, assuming an in-cylinder temperature variation from 300 K to 3000 K, the resonant frequency limits for the different modes are shown in table 2.

Table 2. Bessel constants and resonance frequency for different resonance modes.

Mode (i,j)	Bessel constant $B_{i,j}$	Fr [kHz]
(1,0)	1.841	2.7 – 8.6
(2,0)	3.054	4.5 - 14.2
(0,1)	3.832	5.6 – 17.8
(3,0)	4.201	6.2 – 19.5
(1,1)	5.332	7.8 – 24.8

In [22] Equations (3) and (4) were used to develop an indicator of the resonant energy of the first model. They estimate the theoretical resonance frequency evolution of the first mode and integrate the resonance intensity over that mode by using a given margin of frequencies.

Resonance indicator

The mathematical tool (I_r) presented in [17] is used in this paper to analyze the resonance intensity. The discrete form is defined by:

$$I_r(\alpha) = \sum_{\alpha=\alpha 2}^{\alpha=\alpha 1} w(\alpha-\alpha_1) p_{hp}(\alpha) e^{-2\pi \sum_{\phi=0}^{\phi=\alpha} B\frac{\sqrt{\gamma(\phi)p(\phi)V(\phi)}}{\pi D\sqrt{m}} T(\phi)}\, T(\alpha) \qquad (6)$$

where α_1 and α_2 define the interval where the resonance analysis is performed, w is a window function of $\alpha_1 - \alpha_2$ length, and $T(\alpha)$ is the instantaneous sampling rate, which is constant only in time-based acquisition or if the instantaneous engine speed fluctuations are negligible, B is the Bessel constant, D is the bore of the cylinder, V the chamber volume, m the trapped mass and p the in-cylinder pressure.

This new parametrization offers, not only an indication of the first mode resonance excitation, but also where the mode has been excited without using a computationally expensive time-frequency analysis. For a proper calculation, the in-cylinder pressure signal was filtered with a high-pass filter p_{hp} in order to remove the low-frequency content and the trapped mass was calculated by adding to the measurement of the air mass the injected fuel mass predicted by the ECU.

In the top plot of Figure 3, the high pass pressure evolution of the cycles presented in Figure 2, i.e. a cycle with normal combustion (left), a low knocking cycle (middle), and a high knocking cycle (right), are plotted respect to the distance to the CA50. On the bottom plot, the evolution of the resonance indicator described by Equation (6) and the HRR are also represented, both normalized and respect to the distance to the CA50. Due to the use of a window w to compute the resonance indicator (I_r), the maximum of I_r is delayed from the maximum location of MAPO, this is because the effects on the right and left side affect the transformation.

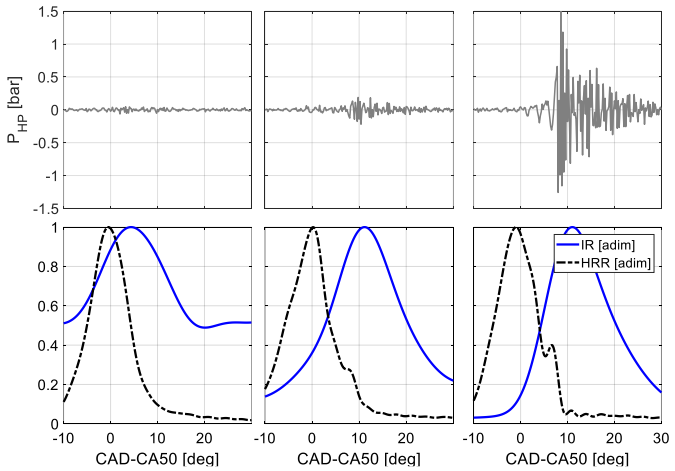

Figure 3. High-pass filtered pressure (top plots) and normalized HRR and I_r (bottom plots) from three cycles at 2000 rpm and 1 bar of intake pressure; no knock (left plots), low knocking cycle (middle plots), and knocking cycle (right plots).

Note that the maximum of the HRR is usually located near the CA50, while the evolution of the indicator I_r depends on how combustion is excited: in the no-knocking cycles (left) resonance is excited during combustion and reaches its maximum between the CA50 and the EOC, while in knocking cycles, although resonance is also excited by normal combustion, the main resonance contribution comes from the auto ignition of the end-gas, at the EOC, and hence, its maximum is found after the EOC.

Knock characterization

As previously mentioned, increasing the spark advance produces higher peak pressure and temperature inside the combustion chamber, and a greater knock probability. The resonance indicator represented by Equation (6) was studied at different engine speeds, spark advance, and load conditions to analyze knocking events at various operating conditions.

The resonance index has been analyzed in two different crank angle position, one at the CA50 (main combustion) and the second one 10 CAD after CA50 (end of combustion), as is shown in figure 4.

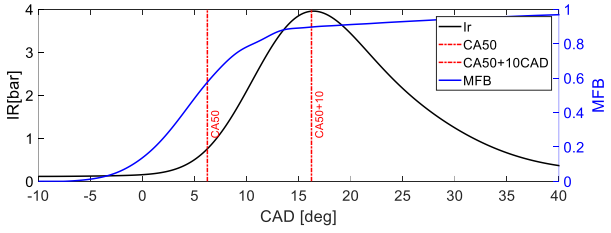

Figure 4. Resonance index and location analysis.

In Figure 5 two datasets of 1000 cycles have been analyzed: both dataset have been collected by running the engine at 2000 rpm and maintaining the intake pressure at 1 bar, but the first dataset (blue histograms) was obtained by stetting the spark advance at 4 CAD-BTDC, i.e. no knocking conditions, while the second one (red histograms) was composed from information of cycles with the SA at 12 CAD-BTDC, therefore with high knocking probability. Furthermore, the value of the I_r at two locations has been studied: in

the left plot, I_r was evaluated at CA50 while on the right plot, the indicator was obtained at 10 CAD after the CA50.

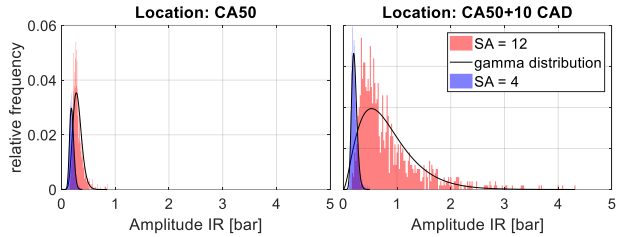

Figure 5. Distribution of the relative frequency of the amplitude of the indicator. (left plot) maximum heat release rate (right plot).

It must be noticed that if we analyze the resonance indicator near the maximum heat release rate (left plot), the range of values obtained will be quite similar in knocking (SA=12 CAD) and no-knocking conditions (SA=4 CAD), but if we analyze the indicator at 10 CAD after the CA50 the differences are notable (right plot). On the one hand, the distributions at the maximum HRR have a small standard deviation in both cases because resonance is excited by the normal combustion and its cycle-to-cycle variation is controlled. The difference in the mean value is due to a sharper combustion process at the SA = 12 CAD. On the other hand, the standard deviation at 10 CAD after the maximum HRR is much higher at the knocking dataset that the one obtained at no knocking conditions, as the auto ignition of the end-gas during knocking cycles leads to higher amplitudes.

Henceforth the maximum amplitude of the resonance indicator, as well as its position seem to be both valuable parameters to characterize the pressure oscillations in a combustion chamber.

In order to characterize knock at each SA, a total of 1000 cycles at six SA settings, namely 4, 5, 8, 10, 11, and 12 CAD-BTDC, have been analyzed. The maximum resonance indicator amplitude and its location, calculated from the CA50, was computed. In figure 6, the frequency in the sense of number of occurrences has been represented with color intensities, being darker colors the most probable locations amplitudes and lighter colors the most unlikely ones.

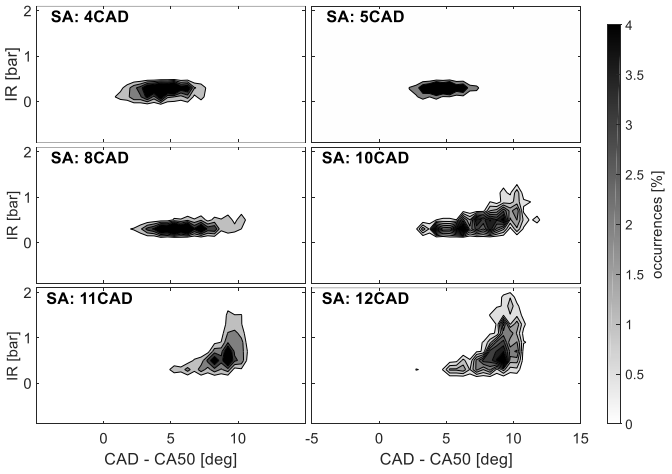

Figure 6. Number of occurrences of the maximum resonance indicator location and amplitude at different SA. 2000 RPM. Pintake:1 bar.

In no knocking cycles, i.e. SA= 4 and 5 CAD-BTDC, the maximum of the resonance indicator is located in a cloud between 2.5 and 7.5 CAD after the CA50, with values below 0.4 bar. This behavior is consistent with normal combustion development where combustion excites resonance in a smooth way.

When spark is advanced before 8 CAD-TDC, an additional cloud located around 10 CAD after CA50, grows up vertically, i.e. varying its intensity. This new could of points represents the knocking events, which are located near the end of combustion and the variability ranges from low intensity values (0.2-0.4 bar) up to high knocking events (>1bar).

When advancing the spark, by maintaining other engine operating parameters constant, not only the percentage of knocking cycles increases, but also the intensity of knocking cycles grows up, as consequence of more fuel burnt in auto ignition combustion. Summarizing, in cycles without knock, i.e. low SA, all the maximums of the resonance indicator are located near the CA50 with low amplitude, while cycles with higher knock probability (advanced SA), the maximums of the resonance indicator are located some degrees after CA50 with a diverse range of intensity.

New knock event definition

In order to determine the minimum oscillation in which it occurs auto ignition of the end gas, the heat release is analyzed. The first law of thermodynamics can be written as [3]:

$$Q = \frac{\gamma - 1}{\gamma} pdV + \frac{1}{\gamma - 1} Vdp \quad (7)$$

where Q is the evolution of the heat in the combustion chamber, p the in-cylinder pressure, γ the specific heat capacities ratio, which commonly ranges from 1.2 to 1.4, and V the instantaneous volume of the combustion chamber, which can be derived from geometrical data of the engine.

Knocking intensity depends on the pressure rise rate due to the spontaneous ignition of the end gas, which can be considered as an instantaneous, therefore constant volume combustion [23], and the heat released by the fuel (Q_f) can be calculated as:

$$Q_f = m_f Hp \quad (8)$$

where Hp is the calorific value of the fuel (45 MJ for gasoline), and m_f the fuel mass burnt.

From (7) and (8), if we assume no wall heat transfer and complete combustion, we can write the difference of pressure at constant volume combustion as:

$$dp = \frac{\gamma - 1}{V} m_{fa} Hp \quad (9)$$

where m_{fa} is the mass fuel burnt in auto-ignition conditions at the end-gas, which is the fuel remaining from the main combustion when knock occurs. Following:

$$m_{fa} = m_f (1 - MFB) \quad (10)$$

where MFB is the mass fraction burnt by the flame front evolution of the SI combustion, i.e. if autoignition takes place at CA90, 10% of

the total fuel would be autoignited, while if autoignition takes place at CA98 only a 2% will be burnt in this mode.

If we consider that the knock resonance excitation is proportional to the sudden rise of the auto ignition event, it is possible to express the auto ignition resonance excitation as a function of the mass fraction burnt, the in-cylinder pressure, the instantaneous volume, and the fuel mass injected, such as:

$$I_{r\_minimum} = G\frac{\gamma - 1}{V} m_f Hp(1 - MFB) \quad (11)$$

where G is the transference constant of excitation of the resonance modes due to the rise of pressure because of the auto ignition.

The mass fraction burnt, can be calculated with the so named apparent heat release, which consists on an estimation of the heat released by the fuel by assuming no wall heat transfer and substituting γ for a constant parameter (κ), following:

$$HRR \approx \frac{\kappa-1}{\kappa} pdV + \frac{1}{\kappa-1} Vdp \quad (12)$$

which indeed converges to a polytrophic process when no heat is released. The mass fraction burnt can be approximated as:

$$MFB(\alpha) = \frac{\int_{\alpha_{SOC}}^{\alpha} HRR(\alpha)\, d\alpha}{\int_{\alpha_{SOC}}^{\alpha_{TOC}} HRR(\alpha)\, d\alpha} \quad (13)$$

These simplifications allow an estimation of the MFB with just the in-cylinder pressure sensor recorded in crank angle base, as the instantaneous volume can be estimated from the crank angle evolution and κ can be approximated by 1.3. However, some uncertainties are expected, specially near the EOC, where the wall heat transfer is higher, and the heat released smaller.

Theoretically, Equation (11) can be used to determine which is the expected intensity from an auto ignition of the end-gas in a given crank angle location. If the auto ignition is produced at the beginning of the combustion a huge resonance intensity is expected, as almost all the fuel will be burnt at knock, but at the end of combustion the expected intensity would be much lower. A limit on the estimated MFB is required for avoiding knock detections when the MFB is reaching the EOC, this limit has been settled at 95% to avoid the MFB errors at the end of the combustion and reject the noises of other sources. If a lower limit was chosen, for example 99%, because MFB is approximate, noise could be confused with low knock.

As a summary, if the maximum resonance indicator (I_r) is greater than the expected resonance at the angle where the indicator is maximum knock is detected:

$$if\ \max(I_r) \geq I_{r_{minimum}}(\alpha_{\max Ir}) \quad knock \quad (14)$$

Figure shows the resonance indicator evolution with a black line, together with the threshold obtained by using a G of 0.08, which was previously calibrated for this engine, in Equation (11) with a dashed red line for the same three cases shown in Figure 3 (no knock, low knock, and knock).

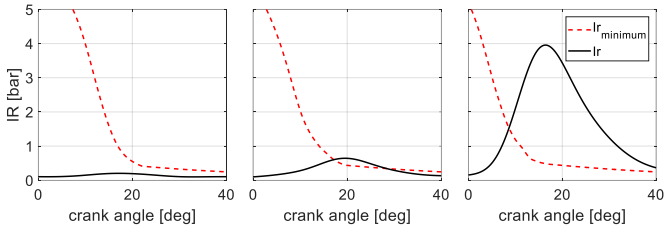

Figure 7. Resonance indicator evolution and auto ignition threshold for a no knock cycle (left plot), low knock cycle (middle plot), and a knock cycle (right plot).

Note than for low and knocking cycles (middle and right plot) the maximum value of the indicator (*Ir*) is higher than the expected resonance at the angle where the indicator is maximum, otherwise for no knocking cycle (left plot) it is lower.
The same analysis was performed in Figure 8, where is plot the highest of the resonance indicator (*Ir*) versus its location of 300 cycles when settling the SA at 11 CAD-BTDC. Black crosses have been used to highlight the cycles where knock is detected with the new knock definition, grey dots represent those cycles that are considered normal combustion, while red circles were added to the cycles that have a MAPO above 0.4 bar (conventional knock characterization). Three cases have been marked with blue circles and have been represented in the right side to illustrate the advantage of the new knock definition: Point number 1 is not classified as knocking for a MAPO threshold of 0.4 bar and has high amplitude of the resonance indicator, while point number 2 and 3 have similar amplitude of the resonance indicator but at different location which makes the difference at the knock criteria. Notice that knock is also evidenced with the peak at the HRR (represented with a red line in the plots at the right side) and that point number 3, which is a low-knocking cycle with MAPO = 0.13 bar, is identified as knock thanks to the new knock event criteria.

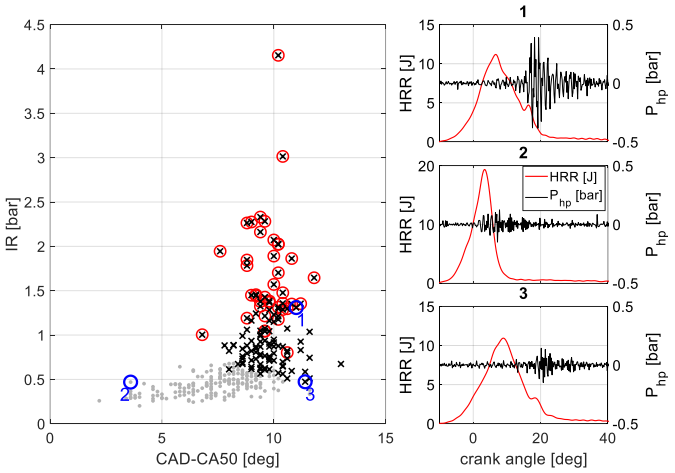

Figure 8. In the left side, the maximum of the resonance indicator versus its location for 300 cycles at 2000 rpm, 1 bar of p_{int}, and 11 CAD-BTDC of SA, where the new knock event definition, marked with crosses, is compared with classical MAPO criteria, marked with red circles. Detailed points are marked with blue circles and zoomed at the right side.

Various steps of SA were performed in order to compare the classical knock definition based on a MAPO threshold with the new knock event definition at various knocking conditions. Figure 9 compares the percentage of knocking cycles obtained from various knock detection criteria at each dataset. Three MAPO threshold were

chosen, two low, at 0.1 bar and 0.2 bar, in order to detect low knocking cycles, and the second one at 0.4 bar to represent a normal knock criterion. As shown in Figure 9, when MAPO threshold is set at 0.1 bar and 0.2, knock events are detected at no knocking conditions, i.e. low values of SA, while if MAPO threshold is 0.4 only high knock events are detected, i.e. the percentage of knocking cycles is lower than the obtained from the new knock event indicator.

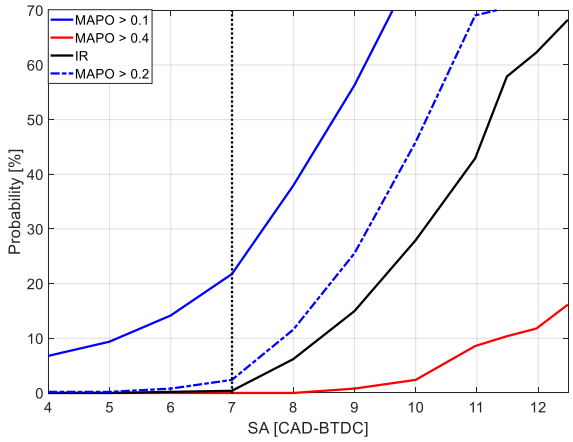

Figure 9. Knock probability for different SA. 2000 rpm. 1 bar intake pressure.

Figure 10 represents the knock probability of the new knock event definition versus the classical definition with a MAPO threshold at 0.4 bar. The SA value is represented by using different color intensities.

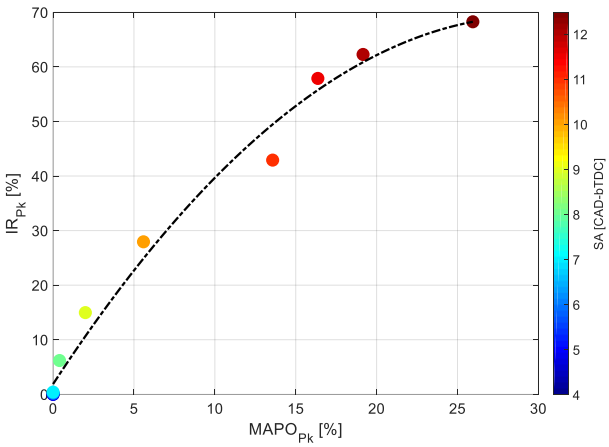

Figure 10. Knock probability for new knock event definition compared with knock probability for MAPO threshold 0.4 bar. 2000 RPM. 1 bar intake pressure. R^2=0.987.

Note that the new definition is capable of recognizing cycles with low knock, being the knock probability greater for each SA, and also that both methods coincide at SA settings where no knock events are identified (SA< 8 CAD-BTDC). The main advantage of being able to detect low knocking cycles and setting the controller with a higher probability than in MAPO case, can be avoided areas where the knock become critical.

A summary of the mean value of percentage of knocking cycles at various operating conditions is given in Table 3. Here the knock detection for MAPO set at 0.4 bar (Pk_{MAPO}) can be compared with the new indicator (Pk_{IR}). More detail information about results summarized in Table 3 can be found in Appendix C.

Table 3. Knock probability for 1500,2000 and 3000 RPM and 0.9,1 and 1.1 bar of intake pressure.

RPM		**1500**			**2000**			**3000**	
Pint [bar]	0.9	1	1.1	0.9	1	1.1	0.9	1	1.1
Pk_{MAPO} [%]	6.2	8.3	0.79	5.9	3	5.2	0.86	4.8	1.98
Pk_{IR} [%]	41	37	4.9	49	9.34	56	4.5	16.4	15.94

Experimental validation

The proposed knock indicator has been implemented in real time with a conventional knock controller. This controller is characterized by adjusting the spark angle $SA_{(i+1)}$ of the forthcoming cycle according to the outcome of the previous firing as:

$$SA_k = \begin{cases} SA_{k-1} - K_{ret} \;\; if \;\; knock \\ SA_{k-1} + K_{adv} \;\; otherwise \end{cases} \tag{15}$$

where k denotes the cycle number, and K_{adv}, K_{ret} are controller gains. K_{ret} is much larger than K_{adv} so the spark slowly advances during non-knocking periods, but it is rapidly retarded if a knock event occurs. These two gains are related by the knock probability, as following:

$$K_{ret} = \frac{1 - p_k}{p_k} K_{adv} \tag{16}$$

The relation between K_{adv} and K_{ret} defines the percentage of knocking cycles while the value of K_{adv} characterize the time response of the controller: on the one hand, high values might allow the controller to reach the optimal value faster when its far from it, but on the other hand the variation of the SA will be higher and hence, higher knock intensities are also expected.

For validation purposes, two tests are shown for MAPO definition at two different thresholds, and two tests for the new definition. For determining the capacities of both definitions to maintain knock at minimum levels and for comparison purposes a value of 0.6% for the MAPO criterion and a value of 2% for the new one have been selected. Table 4 summarizes the characteristics of both controllers.

The response of the controller for each test previously defined is shown in Figure 11. The top plot shows the data obtained from the slow controller while the bottom plot shows the behavior of the fast controller. A dashed black line represents the SA variation when using the MAPO definition at two different thresholds, while a

continuous blue line shows the SA when using the new definition.

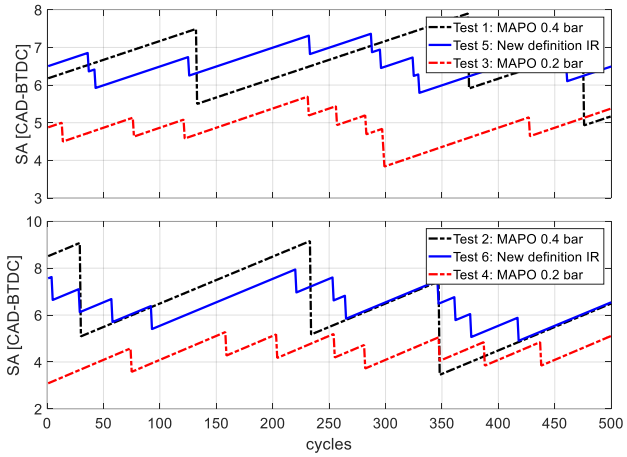

Figure 11. SA control output using MAPO and IR definition. Test 1 and 3 with controller K_{adv}=0.01 (top plot). Test 2 and 4 with controller K_{adv}=0.02 (bottom plot).

For each test the probability of knock for MAPO and the new indicator, the mean SA, its standard deviation, the mean MAPO and its maximum value over 500 cycles were calculated. All the values are in Table 4.

Table 4. Results from test performed with conventional knock controller.

Control Definition	**MAPO 0.4 bar**		**MAPO 0.2 bar**		**New definition IR**	
	Test 1	Test 2	Test 3	Test 4	Test 5	Test 6
K_{adv} [CAD]	0.01	0.02	0.01	0.02	0.01	0.02
K_{ret} [CAD]	1.99	3.98	0.5	1	0.49	0.98
p_{kmapo} [%]	0.6	0.6	2	2	0	0.2
p_{kIR}[%]	2	2	0.5	0.8	2	2.19
Sa_{mean} [CAD]	6.6	6.37	4.87	4.39	6.59	6.39
σ_{SA}	0.66	1.44	0.37	0.45	0.38	0.7
$MAPO_{mean}$ [bar]	0.103	0.106	0.093	0.095	0.102	0.104
$MAPO_{max}$ [bar]	0.783	1.411	0.27	0.23	0.399	0.406
$IMEP_{mean}$ [bar]	11.62	11.60	10.31	10.42	11.59	11.63
σ_{IMEP}	0.158	0.141	0.25	0.24	0.115	0.122

Analyzing Table 4, all the tests have similar knocking conditions as the probability of knock for the new definition for all tests is around 2%. When comparing both definitions with the same controller speed, i.e. tests 1 vs 5 and test 2 vs 6, a similar average value of SA is found, which is consistent with the fact that the final knocking events are quite similar. However, the variability of the SA is almost the double in the classical knock definition. That higher variability makes the knock controller modify the SA to more advanced values leading to dangerous knocking events. The maximum MAPO at tests 5 and 6 (with the new definition) were 0.399 and 0.411 bar, while the maximum MAPO when using the classical definition (tests 1 and 2) were 0.783 and 1.411.

On the other hand, the chosen level of MAPO is lower, and we compare tests 3 vs 5 and test 4 vs 6, the average value of SA in MAPO case is more than 1 CAD for both cases, and the mean value of the IMEP is lower which reduces efficiency.

As a summary, the new knock event definition gives more information about knock, which implies less dispersion at the SA when using a classical knock controller. Regardless of the improvements in drivability and combustion efficiency of the SA variability reduction, a more concise SA control avoids higher SA values which might lead to undesirable MAPO levels.

Conclusions

A knock indicator which take into account the intensity of the oscillations of the in cylinder and its angular evolution is presented in this work and a new definition of knock event is proposed. The minimum oscillation required for the end gas auto ignition detection is based on the constant volume combustion of the fuel mass that is not burnt by the SI flame development.

The method was online validated with the engine running at 2000 rpm and 1 bar of intake pressure, and a conventional knock control algorithm was used for comparing the new knock event definition with the classical MAPO definition. The validation was performed for two different controller speeds, being able to improve the performance of the controllers by giving more information about knock and introducing lower SA variability, which implies a significant reduction of the maximum MAPO reached.

Future work is dedicated to implementing the knock detection method presented along with an adaptive control strategy, to ensure a low percentage of detonation cycles and avoid a continuous variation of SA control.

References

1. Zhen, X., Wang, Y., Xu, S., Zhu, Y., Tao, C., Xu, T., & Song, M. The engine knock analysis–An overview. *Applied Energy*, 92, 628-636, (2012).
2. Wang, Z., Liu, H., & Reitz, R. D. Knocking combustion in spark-ignition engines. *Progress in Energy and Combustion Science*, 61, 78-112. (2017).
3. J.B. Heywood, Internal Combustion Engine Fundamentals, McGraw-Hill, Inc., 1988
4. Bi, F., Ma, T., & Wang, X. Development of a novel knock characteristic detection method for gasoline engines based on wavelet-denoising and EMD decomposition. *Mechanical Systems and Signal Processing*, 117, 517-536, (2019).
5. Shen, X., & Shen, T. Real-time statistical learning-based stochastic knock limit control for spark-ignition engines. *Applied Thermal Engineering*, 127, 1518-1529, (2017).
6. Parra, A. F. S., & Torres, A. G. D. Improvement of a knock model for natural gas SI engines through heat transfer

evaluation. *International Journal on Interactive Design and Manufacturing* (IJIDeM), 12(4), 1423-1433, (2018).
7. Wang, Z., Liu, H., & Reitz, R. D. Knocking combustion in spark-ignition engines. *Progress in Energy and Combustion Science*, 61, 78-112. (2017).
8. Galloni, Enzo. "Knock-limited spark angle setting by means of statistical or dynamic pressure based methods." Energy conversion and management 116 (2016): 11-17.
9. Shu, Gequn, Jiaying Pan, and Haiqiao Wei. "Analysis of onset and severity of knock in SI engine based on in-cylinder pressure oscillations." Applied Thermal Engineering 51.1-2 (2013): 1297-1306.
10. Brecq, G., Bellettre, J., & Tazerout, M. A new indicator for knock detection in gas SI engines. *International Journal of Thermal Sciences*, *42*(5), 523-532, (2003).
11. Galloni, E. Dynamic knock detection and quantification in a spark ignition engine by means of a pressure based method. *Energy conversion and management*, *64*, 256-262,(2012).
12. Parra, A. F. S., & Torres, A. G. D. Improvement of a knock model for natural gas SI engines through heat transfer evaluation. *International Journal on Interactive Design and Manufacturing (IJIDeM)*, *12*(4), 1423-1433, (2018).
13. Gerardin, R. C., Alves, M. A. F., & de França Arruda, J. R. *Analysis of Spark Ignition Engine Knock Signals Using Fourier and Discrete Wavelet Transform* (No. 2009-36-0312). SAE Technical Paper, (2009).
14. Park, S. T., & Yang, J. Engine knock detection based on wavelet transform. In *Proceedings. The 8th Russian-Korean International Symposium on Science and Technology, 2004. KORUS 2004.* (Vol. 3, pp. 80-83). IEEE, June 2004, June.
15. Akimoto, K., Komatsu, H., & Kurauchi, A. Development of pattern recognition knock detection system using short-time Fourier transform. *IFAC Proceedings Volumes*, *46*(21), 366-371, (2013).
16. Bares, P., Selmanaj, D., Guardiola, C., & Onder, C. A new knock event definition for knock detection and control optimization. Applied Thermal Engineering, 131, 80-88, (2018).
17. Guardiola, C., Pla, B., Bares, P., & Barbier, A. An analysis of the in-cylinder pressure resonance excitation in internal combustion engines. *Applied energy*, *228*, 1272-1279.
18. Zhao, K., & Shen, T. Normal-gamma distribution–based stochastic knock probability control scheme for spark-ignition engines. *Proceedings of the Institution of Mechanical Engineers, Part D: Journal of Automobile Engineering*, 0954407019872649, (2019).
19. Bares, P., Selmanaj, D., Guardiola, C., & Onder, C. Knock probability estimation through an in-cylinder temperature model with exogenous noise. *Mechanical Systems and Signal Processing*, *98*, 756-769, (2018).
20. Draper, C. S. (1938). Pressure waves accompanying detonation in the internal combustion engine. *Journal of the Aeronautical Sciences*, *5*(6), 219-226, (2018).
21. Lapuerta M., Armas O. and Hernandez J. J. \Diagnosis of DI Diesel combustion from in-cylinder pressure signal by estimation of mean thermodynamic properties of the gas".Applied Thermal Engineering, Vol. 19 no 5, pp. 513{529, 1999.
22. Shen, X., Zhang, Y., & Shen, T. Cylinder pressure resonant frequency cyclic estimation-based knock intensity metric in combustion engines. *Applied Thermal Engineering*, *158*, 113756. (2019).
23. McKenzie, J., & Cheng, W. K. *The anatomy of knock* (No. 2016-01-0704). SAE Technical Paper, (2016).

Contact Information

Corresponding author: Pau Bares Moreno. Address: CMT-Motores Térmicos, Building 6D, Universitat Politècnica de València,Camino de Vera s/n, 46022 Valencia, Spain.
pabamo@mot.upv.es

Acknowledgments

Irina A. Jimenez received a funding through the grant 132GRISOLIAP/2018/132 from the Generalitat Valenciana and the European Social Fund.

Definitions/Abbreviations

SI	Spark ignition engine
SA	Spark advance
MAPO	Maximum Amplitude of Pressure Oscillations
IMPO	Integral of Modulus of Pressure Oscillations
EOC	End of Combustion
ECU	Electronic control unit
VGT	Variable geometry turbine
VVT	Variable valve timing
n	Engine Speed
Sn	Sampling accuracy
p	In-cylinder pressure
CAD	Crank angle degree
BTDC	Before top dead center
IMEP	Indicated mean effective pressure
HRR	Heat release rate
CA50	location of the crank angle position where 50% of the heat is released
Pk	Knock probability
TDC	Top dead center
MFB	Mass fraction burnt
STFT	Short-time Fourier transform
IR	Resonance indicator

Appendix A

In this appendix the difference between the in-cylinder pressure signal and the knock sensor for low knocking cycles detection is analyzed. Figure A1 shows a no knocking cycle on top plots and a low knocking cycle in bottom plots, on left side the high-pass in-cylinder pressure signal is plotted and the HRR, and on right side the high-pass knock sensor signal its plotted.

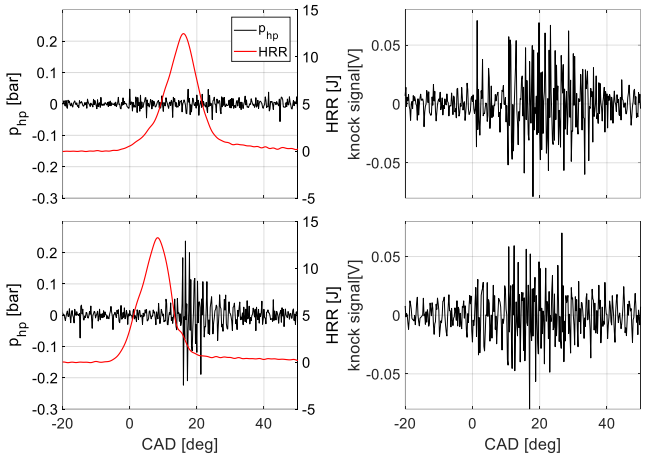

Figure A1. (Top plots) No-knocking cycle. (bottom plots) low-knocking cycle.
(left plots) High-pass in-cylinder pressure and HRR. (right plots) High-pass knock sensor signal.

Notice that in the case of a no knocking cycle MAPO from knock sensor is 0.07, and for a low knocking cycle is around the same value.
In figure B2 in the left plot, MAPO from the knock sensor is represented over 1000 cycles. Red crosses have been used to highlight the cycles where knock is detected with knock in-cylinder pressure (MAPO>0.3 bar). Three cases have been marked with blue circles and represented in the right side.

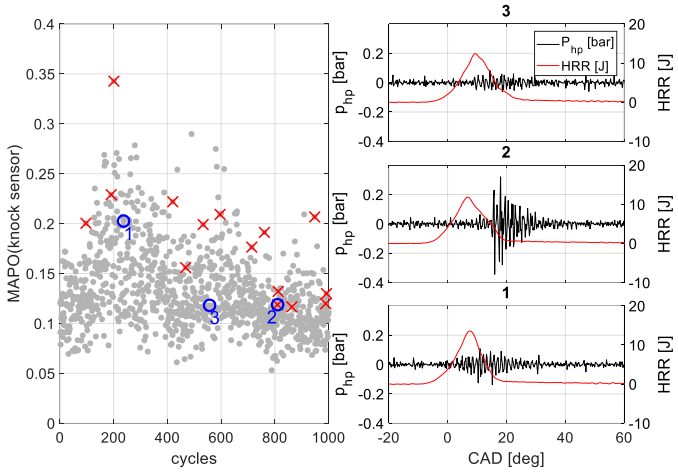

Figure A2. (left plots) MAPO from knock sensor over 1000 cycles. (left plots) High-pass in-cylinder pressure and HRR for three marked cases.

Cases 3 and 2 has the same MAPO from knock sensor, while MAPO obtain from the in-cylinder pressure is different. Case 2 is a low knocking cycle, while case 3 is normal combustion. In case 1, MAPO from knock sensor is higher, while is clearly a no-knocking cycle. Note that in-cylinder pressure has more information about low-knocking cycles, for this reason it is widely used in research laboratory for calibration [10].

Appendix B

The STFT consists on breaking up the signal and separately analyses each piece of the signal. Windows are used in harmonic analysis to reduce the undesirable effects related to spectral leakage. There are several different types of window functions that can be apply depending on the signal, three examples are shown in figure B1 left plot.

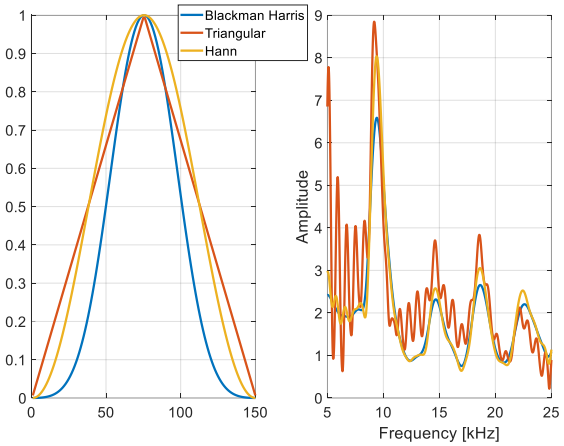

Figure B1 (left plot) Blackman Harris, Hamming and Triangular windows shape.
(right plot) Effect on FFT with different type of windows

The Blackman Harris and Hann window functions both have a sinusoidal shape, and result in a wide peak but low side lobes touching zero at both ends eliminating all discontinuity. Triangular window does not reach zero and thus still has a slight discontinuity in the signal. In figure B1 right plot this effect is shown, the fast Fourier transform for the in-cylinder pressure in 14 CAD is performed for the three windows plotted in the left plot, for Blackman Harris and Hann windows cases the amplitude for each frequency has a smooth shape than in the other case.

Appendix C

In this appendix the table 3 of the section New knock event definition is expanded. In plot C1 is represented for the different intake pressure knock probability for new knock event definition (IR_{pk}) compared with knock probability for MAPO threshold 0.4 bar ($MAPO_{pk}$), in different color are marked the different RPM and the intensity of color represents the spark advance of each case.

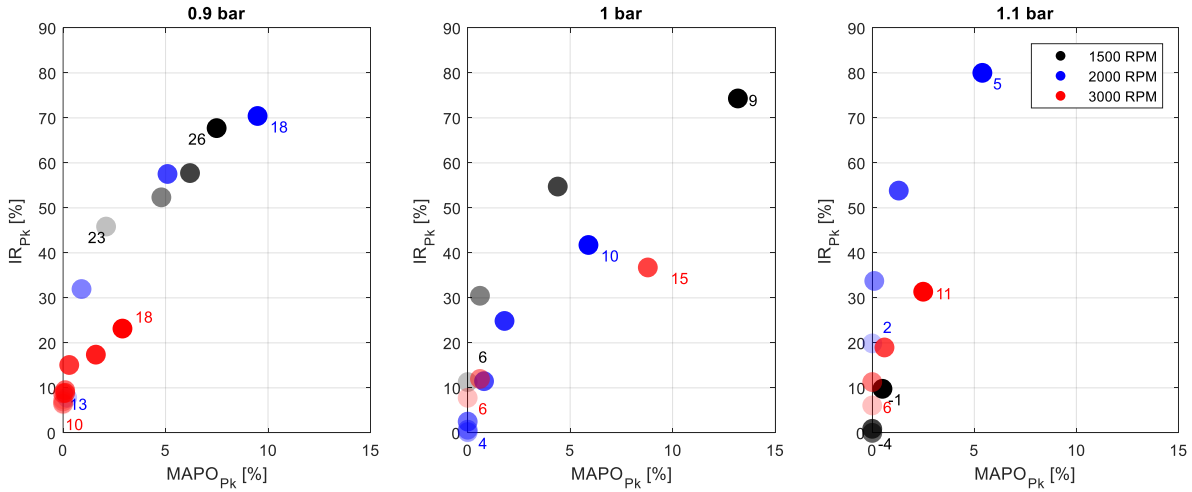

Figure C1. Knock probability for new knock event definition compared with knock probability for MAPO threshold 0.4 bar. (left plot) 0.9 bar (middle plot) 1 bar. (right plot) 1.1 bar

Notice that in the case of 0.9 bar, the influence of the RPM in 3000 RPM is notable, less knock cases are found for both of the indicators. While for 1500 RPM and 2000 RPM knocking cycles follow the same tendency. In 2000 RPM in cases with lower RPM (1500), more knocking cycles are found, while this decrease when RPM increase. And in the last case, 1.1 bar, 2000 RPM case the probability pf low knocking cycles increases faster than 1500 RPM and 3000 RPM.